

Analytical models of plane turbulent wall-bounded flows

Victor L. Mironov and Sergey V. Mironov

Institute for Physics of Microstructures, Russian Academy of Sciences,
GSP-105, Nizhny Novgorod, 603950, Russia

e-mail: mironov@ipmras.ru

July 11, 2023

Abstract

We present the theoretical description of plane turbulent wall-bounded flows based on the previously proposed equations for vortex fluid, which take into account both the longitudinal flow and the vortex tubes rotation. Using the simple model of eddy viscosity we obtain the analytical expressions for mean velocity profiles of steady-state turbulent flows. In particular we consider near-wall boundary layer flow as well as Couette, Poiseuille and combined Couette-Poiseuille flows. In all these cases the calculated velocity profiles are in good agreement with experimental data and results of direct numerical simulations.

1 Introduction

The plane wall-bounded flows are relatively simple types of shear flows, which are actively investigated both theoretically and experimentally for a long time. Conventionally, the studies in this area can be divided into four groups: near-wall (boundary layer) flow [1]-[5], Couette flow [6]-[12], Poiseuille flow [13]-[15], and combined Couette-Poiseuille flow [16]-[19]. In particular, the special attention is paid to the conditions for the transition to the turbulent regime and the dependence of the parameters of a steady turbulent flow on the Reynolds number (Re) and on the boundary conditions on the walls. The theoretical description of turbulent flows is based on the solution of the Reynolds-averaged Navier–Stokes (RANS) equation with the Reynolds stress tensor, which takes into account the influence of the fluctuating part of the velocity on the average flow characteristics [20],[21]. There are several approaches to calculating the Reynolds tensor and closing the system of equations for a turbulent flow [22]-[25]. The central point here is the concept of eddy viscosity, which relates fluctuating velocities to the average flow velocity. It is assumed that the eddy viscosity depends on the coordinates in the flow, which makes it possible, using additional boundary layer models, to match the results of calculations with experimental data [26]-[28]. With the development of computer technology, methods for the direct numerical simulations (DNS) based on solution of non-stationary RANS equation have become widespread. These methods allow one to simulate the evolution of unsteady flows and calculate the average values of different physical quantities [29]-[33].

The existing analytical models of turbulence adequately describe the experimental data, however, they contain many fitting parameters and are difficult for analysis. The advantages and disadvantages of various models are considered in [34],[35]. They satisfactorily describe the experimental distributions of mean velocity in the central region of the flow, however the matching of the velocity profiles near the walls require additional assumptions related to the properties of the eddy viscosity in this region. Therefore, there is still a need for a simple analytical model suitable for the estimations and simple explanation of experimental results.

In this paper, we consider the description of a turbulent flow based on a symmetric system of equations explicitly accounting vortex motion. There are a number of works in the literature, in which a symmetric system of Maxwell-type equations for the velocity and the vorticity vectors is used to describe the vortex flow [36]-[42]. In particular, these equations are applied for the consideration of turbulent flows [39] and electron-ion plasma in the framework of a hydrodynamic two-fluid model [43]-[45]. However, the additional equation for vorticity is actually obtained by applying the curl operator to the Euler equation, so the resulting equation is not independent. Recently, we have developed an alternative approach based on the droplet model of a liquid, which was introduced by Helmholtz [46]. We have derived a system of Maxwell-type equations, which take into account the longitudinal motion and rotation of vortex tubes [47]-[49]. In [50], we generalized these equations for the case of turbulent flows. As an example we considered Couette flow in the framework of simple model of eddy viscosity based on Boussinesq assumption [51]-[52] and showed that there is a good agreement between the calculated velocity profiles and experimental data.

In the present paper we apply this approach for the description of near-wall turbulent flows as well as for Couette, Poiseuille and combined Couette-Poiseuille turbulent flows. We derive the analytical expressions for the profiles of mean velocity and demonstrate that they are in good agreement with experimental data and results of direct numerical simulations.

2 Model of vortex plane flow

In the present paper we consider steady-state plane turbulent flows of viscous vortex fluid moving parallel to the plane xy with the velocity directed along the X axis (Fig. 1).

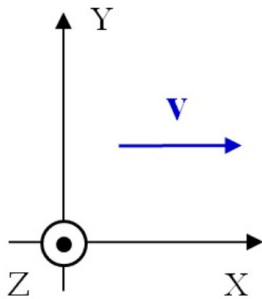


Figure 1: Sketch of the coordinate system for the plane flow. The fluid moves along the X axis with speed v .

As we previously showed [50], in case of incompressible fluid a vortex isentropic flow is described by

the following symmetric equations:

$$\begin{aligned}
\frac{1}{c} \left(\frac{\partial}{\partial t} + (\mathbf{v} \cdot \nabla) - \nu \Delta \right) \mathbf{v} + \nabla \times \mathbf{w} + \frac{1}{c\rho} \nabla p &= 0, \\
\frac{1}{c} \left(\frac{\partial}{\partial t} + (\mathbf{v} \cdot \nabla) - \nu \Delta \right) \mathbf{w} - \nabla \times \mathbf{v} &= 0, \\
\nabla \cdot \mathbf{v} &= 0, \\
\nabla \cdot \mathbf{w} &= 0.
\end{aligned} \tag{1}$$

Here c is a speed of sound, \mathbf{v} is a local velocity, ν is a kinematic viscosity, ρ is a fluid density, p is a pressure. The vector \mathbf{w} characterizes the rotation of the vortex tube around its axis

$$\begin{aligned}
\mathbf{w} &= 2c \boldsymbol{\theta}, \\
\boldsymbol{\omega} &= \frac{d\boldsymbol{\theta}}{dt},
\end{aligned} \tag{2}$$

where $\boldsymbol{\theta}$ is the angular vector of rotation and $\boldsymbol{\omega}$ is the angular velocity of the vortex tube rotation.

To describe the turbulent flow, we represent $\mathbf{v} = \bar{\mathbf{v}} + \mathbf{v}'$, where $\bar{\mathbf{v}}$ is the time-averaged velocity and \mathbf{v}' describes the velocity fluctuations. Similarly, for the tube rotation vector we take $\mathbf{w} = \bar{\mathbf{w}} + \mathbf{w}'$. Considering plane flow we assume that the velocity \mathbf{v} has only x component and depends only on the y coordinate $v_x = v_x(y, t)$. Similarly, in plane flow the vector of rotation angle \mathbf{w} has only z component and depends only on y coordinate $w_z = w_z(y, t)$. Also we assume that $\frac{1}{c\rho} \frac{\partial p}{\partial x} = -g = \text{const}$. Then for the time averaged values we obtain the following equations

$$\begin{aligned}
\frac{1}{c} \frac{\partial \bar{v}_x}{\partial t} - \lambda \frac{\partial^2 \bar{v}_x}{\partial y^2} + \frac{\partial \bar{w}_z}{\partial y} - g &= 0, \\
\frac{1}{c} \frac{\partial \bar{w}_z}{\partial t} - \lambda \frac{\partial^2 \bar{w}_z}{\partial y^2} + \frac{\partial \bar{v}_x}{\partial y} &= 0,
\end{aligned} \tag{3}$$

where the parameter λ is a constant characterizing the scale of the turbulence. This parameter is defined by eddy viscosity [50]. In the next sections, we consider some simple solutions to this system for various cases of plane turbulent flows.

3 Near-wall turbulent flow

Let us consider a steady-state turbulent flow near the infinite plate (Fig. 2) without pressure gradient ($g = 0$).

First we consider the case when, on average, the steady flow occurs at zero value of the average angular velocity of the vortex tubes ($\bar{\boldsymbol{\omega}} = 0$). The values \bar{v}_x and \bar{w}_z depend only on the y coordinate and do not depend on time $\bar{v}_x = \bar{v}_x(y)$, $\bar{w}_z = \bar{w}_z(y)$. Then the equations (3) take the following form:

$$\begin{aligned}
-\lambda \frac{\partial^2 \bar{v}_x}{\partial y^2} + \frac{\partial \bar{w}_z}{\partial y} &= 0, \\
-\lambda \frac{\partial^2 \bar{w}_z}{\partial y^2} + \frac{\partial \bar{v}_x}{\partial y} &= 0.
\end{aligned} \tag{4}$$

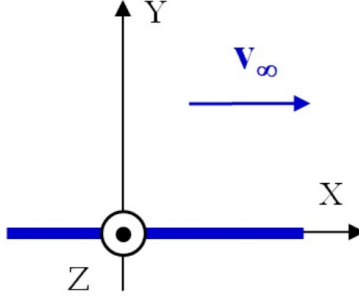


Figure 2: Sketch of the fluid flow along the X axis with speed v_∞ over the infinite plate.

The boundary conditions for the velocity are

$$\begin{aligned}\bar{v}_x(0) &= 0, \\ \bar{v}_x(\infty) &= v_\infty.\end{aligned}\tag{5}$$

The boundary conditions for the rotation angle $\bar{w}_z(y)$ are not obvious, therefore we choose them in the following form

$$\begin{aligned}\bar{w}_z(0) &= w_0, \\ \bar{w}_z(\infty) &= w_\infty,\end{aligned}\tag{6}$$

where w_0 and w_∞ are certain values.

The solutions of system (4) are written as

$$\bar{v}_x = v_\infty \{1 - \exp(-y/\lambda)\},\tag{7}$$

$$\bar{w}_z = -v_\infty \{1 - \exp(-y/\lambda)\} + w_0.\tag{8}$$

The values w_0 and w_∞ satisfy the following relation

$$w_0 - w_\infty = v_\infty.\tag{9}$$

Note that the velocity distribution (7) does not depend on the boundary conditions for the function $w_z(y)$. On the other hand, the angle of rotation is determined up to a constant value. Therefore, without loss of generality, one can choose the beginning of angle counting as $w_0 = 0$.

The normalized distribution of the mean velocity (7) is shown in Fig. 3. Note that since we consider the flows with $v_\infty < c$, the average angle of rotation $\bar{\theta}_z = \bar{w}_z/2c$ is small.

We emphasize that in this case the only spatial scale is the turbulent length λ . However, in theoretical models and in experimental studies, the concept of a turbulent boundary layer is actively used. Therefore, further we consider another model of turbulent flow, in which we artificially introduce an additional spatial scale, namely the boundary layer thickness.

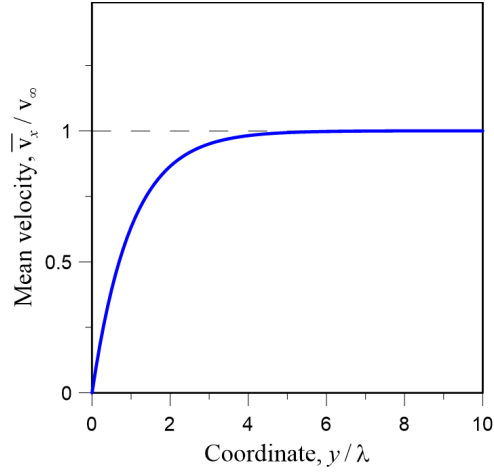


Figure 3: Stationary profile of the mean velocity of turbulent flow over an infinite plate.

4 Flow in the near-wall boundary layer

4.1 Flow in the near-wall layer without tubes rotation

The model of turbulent flow in thin near-wall layer is often used for the interpretation of experimental data. Let us consider the boundary layer with a thickness δ , in which the motion is turbulent, and outside ($y > \delta$) it is laminar with the velocity v_∞ (Fig. 4).

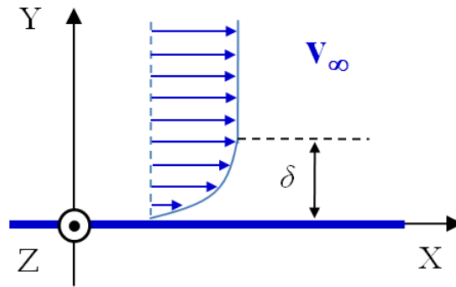


Figure 4: Sketch of a steady-state turbulent flow in a thin layer over an infinite plate.

In the region $0 \leq y \leq \delta$ this flow is described by the system of equations

$$\begin{aligned} -\lambda \frac{\partial^2 \bar{v}_x}{\partial y^2} + \frac{\partial \bar{w}_z}{\partial y} &= 0, \\ -\lambda \frac{\partial^2 \bar{w}_z}{\partial y^2} + \frac{\partial \bar{v}_x}{\partial y} &= 0, \end{aligned} \tag{10}$$

with the following boundary conditions:

$$\begin{aligned}\bar{v}_x(0) &= 0, \\ \bar{v}_x(\delta) &= v_\infty, \\ \bar{w}_x(0) &= w_0, \\ \bar{w}_x(\delta) &= w_\delta,\end{aligned}\tag{11}$$

where w_0 and w_δ are certain constants.

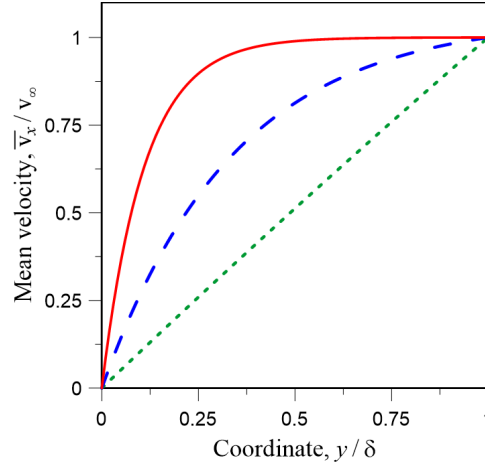


Figure 5: The mean velocity profiles of turbulent flow in the boundary layer for different parameters λ/δ . The green dotted line $\lambda/\delta = 10$; the blue dashed line $\lambda/\delta = 0.34$; the red solid line $\lambda/\delta = 0.11$.

We will look for the solutions to this system under the additional condition that at $\delta \rightarrow \infty$ the solutions have to transform to (7) and (8). The corresponding solutions in the region of the near-wall layer have the following form:

$$\bar{v}_x = v_\infty \frac{1 - \exp(-y/\lambda)}{1 - \exp(-\delta/\lambda)},\tag{12}$$

$$\bar{w}_z = -v_\infty \frac{1 - \exp(-y/\lambda)}{1 - \exp(-\delta/\lambda)} + w_0.\tag{13}$$

The values w_0 and w_δ are related by the following relation:

$$w_0 - w_\delta = v_\infty.\tag{14}$$

Indeed, it is not difficult to see that when $\delta \rightarrow \infty$ the solutions (12) and (13) transform to previous solutions (7) and (8). As an example, Fig. 5 shows several velocity profiles calculated by formula (12) for different parameters λ/δ . Note when $\delta/\lambda \ll 1$ the mean velocity is $\bar{v}_x \simeq v_\infty y/\delta$.

The solution (12) can be used to describe turbulent flows with low Reynolds numbers and for the flows near the leading edge of a flat plate. As an example Fig. 6 demonstrates the fitting of experimental velocity profile near the leading edge [2]. One can see that the calculated profile is in a good agreement with experimental data. For comparison, the same figure shows the Blasius profile for laminar flow, normalized to $0.99 v_\infty$ [53].

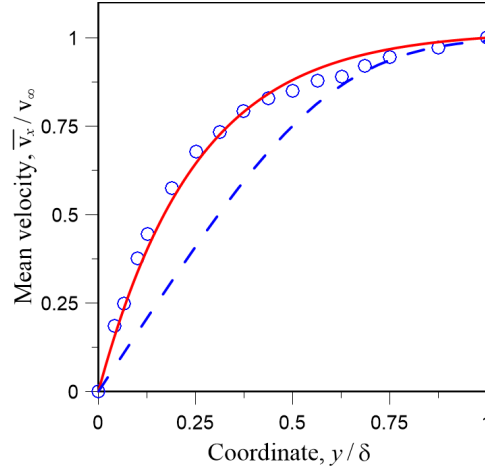


Figure 6: The mean velocity profiles of turbulent flow. The circles (\circ) are the experimental data [2], the solid red line corresponds to the distribution (12) with the parameters $\lambda/\delta = 0.25$. The Blasius profile is shown by dashed line.

4.2 Turbulent flow in the near-wall layer with rotation of vortex tubes

Let us consider a model of turbulent flow in the near-wall layer of thickness δ taking into account the rotation of vortex tubes (Fig. 7). We assume that in average the tubes rotate with the same angular

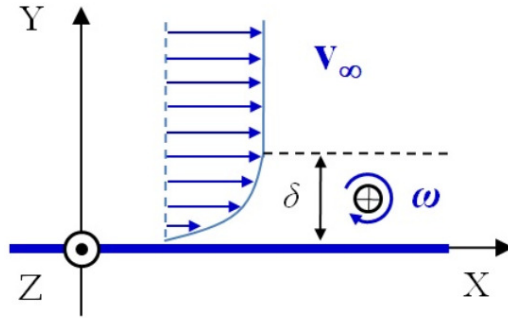


Figure 7: Sketch of stationary turbulent flow over an infinite plate. The vortex tubes in the thin layer, on average, rotate with angular velocity $\bar{\omega}$.

velocity $\bar{\omega}_z$, but with different phases $\bar{\varphi}_z(x)$. Then the vector of rotation is written as

$$\bar{\omega}_z(x, t) = 2c\bar{\omega}_z t + \bar{\varphi}_z(x). \quad (15)$$

In this case the equations (3) take the following form

$$\begin{aligned} -\lambda \frac{\partial^2 \bar{v}_x}{\partial y^2} + \frac{\partial \bar{\varphi}_z}{\partial y} &= 0, \\ -\lambda \frac{\partial^2 \bar{\varphi}_z}{\partial y^2} + \frac{\partial \bar{v}_x}{\partial y} + 2\bar{\omega}_z &= 0. \end{aligned} \tag{16}$$

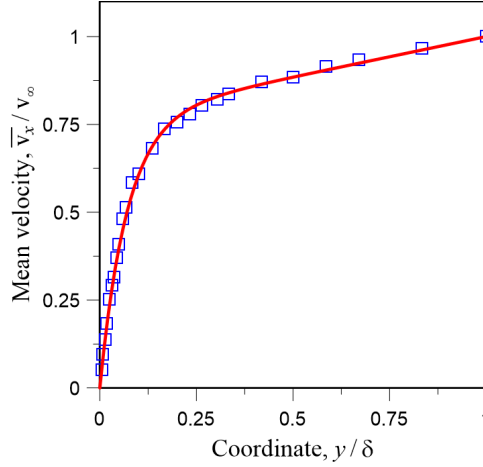


Figure 8: The mean velocity profiles of turbulent flow over a flat fixed wall. The squares (\square) are the experimental data [3], the solid red line corresponds to the distribution (18) with the parameters $\lambda/\delta = 0.071$, $\beta = 0.23$.

We choose the following boundary conditions

$$\begin{aligned} \bar{v}_x(0) &= 0 \\ \bar{v}_x(\delta) &= v_\infty, \\ \bar{\varphi}_z(0) &= \varphi_0, \\ \bar{\varphi}_z(\delta) &= \varphi_\delta. \end{aligned} \tag{17}$$

We will look for the solutions to this system under the additional conditions that at $\omega \rightarrow 0$ and $\delta \rightarrow \infty$ the solutions have to transform to (7) and (8). Then the solution of system (16) in the region of the near-wall layer has the following form:

$$\bar{v}_x = v_\infty(1 - \beta) \frac{1 - \exp(-y/\lambda)}{1 - \exp(-\delta/\lambda)} + v_\infty \beta \frac{y}{\delta}, \tag{18}$$

$$\bar{\varphi}_z = -v_\infty(1 - \beta) \frac{1 - \exp(-y/\lambda)}{1 - \exp(-\delta/\lambda)} + \varphi_0. \tag{19}$$

Here we introduce the dimensionless parameter $\beta = -2\bar{\omega}_z\delta/v_\infty$. The values φ_0 and φ_δ are related by the following relation

$$\varphi_0 - \varphi_\delta = v_\infty(1 - \beta). \tag{20}$$

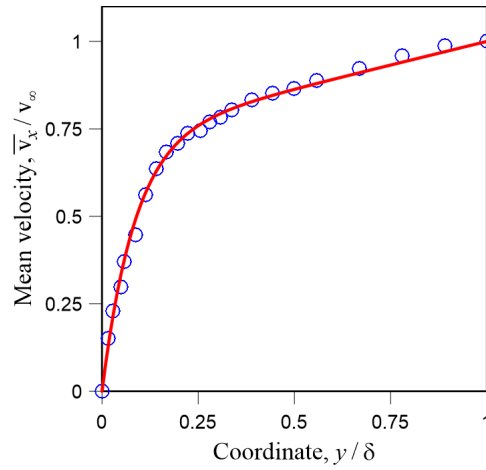


Figure 9: The mean velocity profiles of turbulent flow over a wall with obstacle. The circles (\circ) are the experimental data [2], the solid red line corresponds to the distribution (18) with the parameters $\lambda/\delta = 0.085$, $\beta = 0.27$.

As an example, Fig. 8 shows the fitting of experimental data [3] for turbulent flow over a flat fixed wall using the distribution (18). Fig. 9 demonstrates the calculated and experimental velocity profiles for turbulent flow over a wall with obstacle. These figures show the good agreement between the fitted curves and the experimental data.

5 Turbulent plane Couette flow

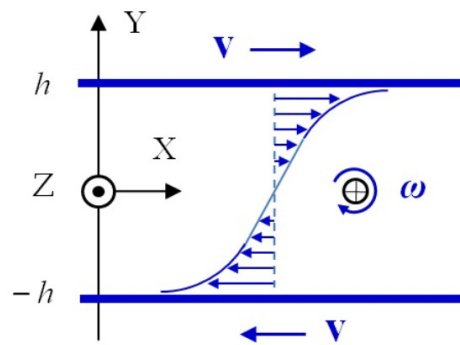


Figure 10: Sketch of a plane Couette flow between two infinite plates, which move along the X axis with speed v in opposite directions.

We consider a turbulent flow of viscous vortex fluid formed between two infinite, parallel plates moving relative to each other in opposite directions with speed v (Fig. 10).

5.1 Couette flow without rotation of vortex tubes

First, we consider a steady-state turbulent flow, when the average angular velocity of the vortex tubes rotation is equal to zero ($\bar{\omega}_z = 0$). This flow is described by equations

$$\begin{aligned} -\lambda \frac{\partial^2 \bar{v}_x}{\partial y^2} + \frac{\partial \bar{w}_z}{\partial y} &= 0, \\ -\lambda \frac{\partial^2 \bar{w}_z}{\partial y^2} + \frac{\partial \bar{v}_x}{\partial y} &= 0. \end{aligned} \quad (21)$$

We choose the following boundary conditions:

$$\begin{aligned} \bar{v}_x(h) &= v, \\ \bar{v}_x(-h) &= -v, \\ \bar{w}_z(h) &= w_h, \\ \bar{w}_z(-h) &= w_{-h}, \end{aligned} \quad (22)$$

where w_h and w_{-h} are certain values.

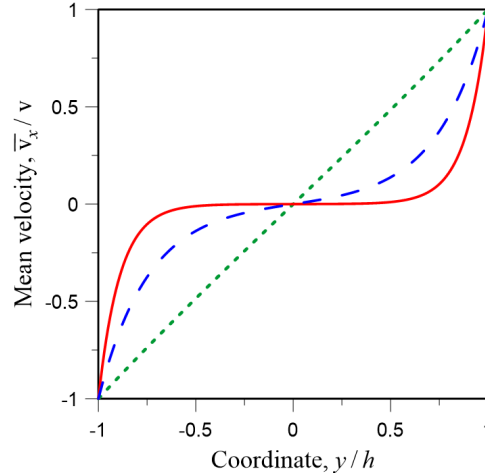


Figure 11: The model profiles of the mean velocity of turbulent Couette flow without rotation of vortex tubes. The dotted green line $\lambda/h = 2$, dashed blue line $\lambda/h = 0.26$, solid red line $\lambda/h = 0.11$.

In this case the solutions satisfying the boundary conditions (22) are

$$\bar{v}_x = v \frac{\sinh(y/\lambda)}{\sinh(h/\lambda)} + \frac{(w_h - w_{-h}) [\cosh(y/\lambda) - \cosh(h/\lambda)]}{2 \sinh(h/\lambda)}, \quad (23)$$

$$\bar{w}_z = v \frac{[\cosh(y/\lambda) - \cosh(h/\lambda)]}{\sinh(h/\lambda)} + \frac{(w_h - w_{-h}) \sinh(y/\lambda)}{2 \sinh(h/\lambda)} + \frac{w_h + w_{-h}}{2}. \quad (24)$$

For the antisymmetric Couette flow $\bar{v}_x(0) = 0$ and, therefore, the angles are related as $w_h = w_{-h}$. In this case the velocity profile is fully antisymmetric

$$\bar{v}_x = v \frac{\sinh(y/\lambda)}{\sinh(h/\lambda)}. \quad (25)$$

As an example, the mean velocity distributions (25) for different parameters λ/h are shown in Fig. 11. Note, that when $h/\lambda \ll 1$ the mean velocity profile is linear $\bar{v}_x \simeq v y/h$.

5.2 Couette flow with vortex tubes rotation

Let us consider fully developed turbulent flow, in which the vortex tubes on average rotate with a constant angular velocity $\bar{\omega}_z = \text{const}$, but with different phases $\bar{\varphi}_z(y)$. We will look for a solution in the following form:

$$\begin{aligned} \bar{v}_x(y, t) &= \bar{v}_x(y), \\ \bar{w}_z(y, t) &= 2c\bar{\omega}_z t + \bar{\varphi}_z(y). \end{aligned} \quad (26)$$

Then the equations (3) take the following form:

$$\begin{aligned} -\lambda \frac{\partial^2 \bar{v}_x}{\partial y^2} + \frac{\partial \bar{\varphi}_z}{\partial y} &= 0, \\ -\lambda \frac{\partial^2 \bar{\varphi}_z}{\partial y^2} + \frac{\partial \bar{v}_x}{\partial y} + 2\bar{\omega}_z &= 0. \end{aligned} \quad (27)$$

As the boundary conditions, we choose

$$\begin{aligned} \bar{v}_x(h) &= v, \\ \bar{v}_x(-h) &= -v, \\ \bar{\varphi}_z(h) &= \varphi_h, \\ \bar{\varphi}_z(-h) &= \varphi_{-h}, \end{aligned} \quad (28)$$

where φ_h and φ_{-h} are certain phases.

The solutions of equations (27) are written as

$$\bar{v}_x = \alpha v \frac{y}{h} + (1 - \alpha) v \frac{\sinh(y/\lambda)}{\sinh(h/\lambda)} + \frac{(\varphi_h - \varphi_{-h}) \cosh(y/\lambda) - \cosh(h/\lambda)}{2 \sinh(h/\lambda)}, \quad (29)$$

$$\bar{\varphi}_z = (1 - \alpha) v \frac{\cosh(y/\lambda) - \cosh(h/\lambda)}{\sinh(h/\lambda)} + \frac{(\varphi_h - \varphi_{-h}) \sinh(y/\lambda)}{2 \sinh(h/\lambda)} + \frac{\varphi_h + \varphi_{-h}}{2}, \quad (30)$$

where we introduce the dimensionless parameter

$$\alpha = -\frac{2\bar{\omega}_z h}{v}. \quad (31)$$

Let us consider fully antisymmetric Couette flow. In this case we assume that $\bar{v}_x(0) = 0$ and, therefore, the phases are related as $\varphi_h = \varphi_{-h}$. Then we obtain the following distribution of velocity

$$\bar{v}_x = \alpha v \frac{y}{h} + (1 - \alpha) v \frac{\sinh(y/\lambda)}{\sinh(h/\lambda)}. \quad (32)$$

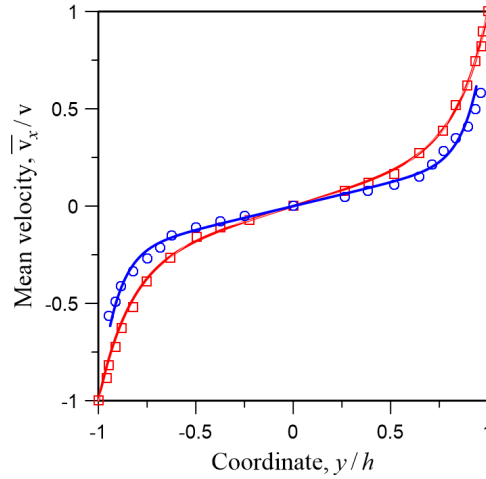


Figure 12: Distributions of the mean-velocity in a turbulent Couette flow. Squares (\square) are the experimental results for $Re = 2900$ [6]; solid red line corresponds to (32) at $\lambda/h = 0.16$, $\alpha = 0.3$. Circles (\circ) are the experimental results for $Re = 18000$ [6]; solid blue line corresponds to (32) at $\lambda/h = 0.09$, $\alpha = 0.24$.

As an example, in Fig. 12 we show the comparison of mean velocity distribution (32) with experimental results for Couette flow with $Re = 2900$ and $Re = 18000$ [6].

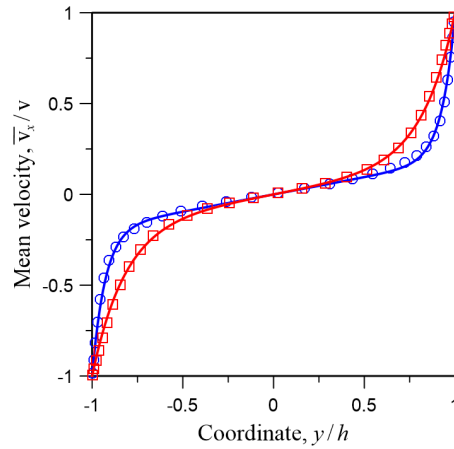


Figure 13: Distributions of the mean-velocity in a turbulent Couette flow between two moving plates. Squares (\square) are the results of DNS with $Re = 3000$ [54]; solid red line corresponds to (32) at $\lambda/h = 0.18$, $\alpha = 0.165$. Circles (\circ) are the DNS results with $Re = 12800$ [55]; solid blue line corresponds to (32) at $\lambda/h = 0.072$, $\alpha = 0.189$.

In addition, Fig. 13 demonstrates the comparison of solution (32) with the DNS results for Couette flow with $Re = 3000$ [54] and $Re = 12800$ [55]. In all cases the fitted velocity profiles are in good agreement with the experimental data and the results of the DNS.

6 Plane turbulent Poiseuille flow

In case of plane Poiseuille flow in a channel with fixed walls (Fig. 14), the fluid moves under the action of a pressure gradient.

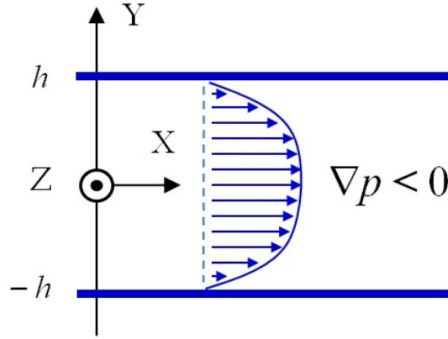


Figure 14: Sketch of a plane turbulent Poiseuille flow in a channel between two infinite plates.

Let us consider a steady-state turbulent flow. In this case the equations (3) take the following form:

$$\begin{aligned} -\lambda \frac{\partial^2 \bar{v}_x}{\partial y^2} + \frac{\partial \bar{w}_z}{\partial y} - g &= 0, \\ -\lambda \frac{\partial^2 \bar{w}_z}{\partial y^2} + \frac{\partial \bar{v}_x}{\partial y} &= 0, \end{aligned} \quad (33)$$

with the following boundary conditions

$$\begin{aligned} \bar{v}_x(h) &= \bar{v}_x(-h) = 0, \\ \bar{w}_z(h) &= w_h \\ \bar{w}_z(-h) &= w_{-h}. \end{aligned} \quad (34)$$

The solutions of system (33) are

$$\bar{v}_x = \frac{(gh - w_h + w_{-h})}{2} \frac{[\cosh(h/\lambda) - \cosh(y/\lambda)]}{\sinh(h/\lambda)}, \quad (35)$$

$$\bar{w}_z = -\frac{(gh - w_h + w_{-h})}{2} \frac{\sinh(y/\lambda)}{\sinh(h/\lambda)} + gh \frac{y}{h} + \frac{w_h + w_{-h}}{2}. \quad (36)$$

The normalized velocity distribution (35) for different parameters λ/h is shown in Fig. 15. The normalization is \bar{v}_x/\bar{v}_0 (where \bar{v}_0 is the velocity at $y = 0$).

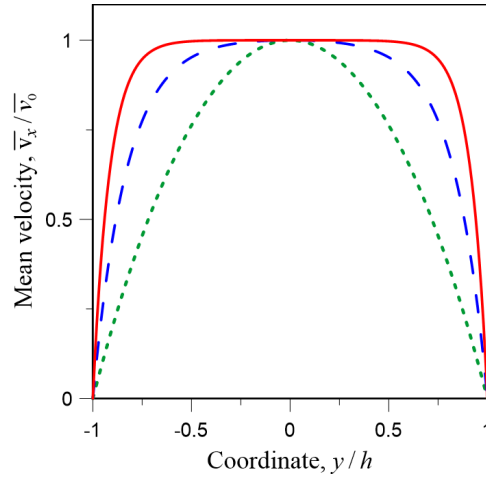


Figure 15: The profiles of the mean velocity of turbulent Poiseuille flow (35). The dotted green line $\lambda/h = 1.1$; dashed blue line $\lambda/h = 0.2$; solid red line $\lambda/h = 0.085$.

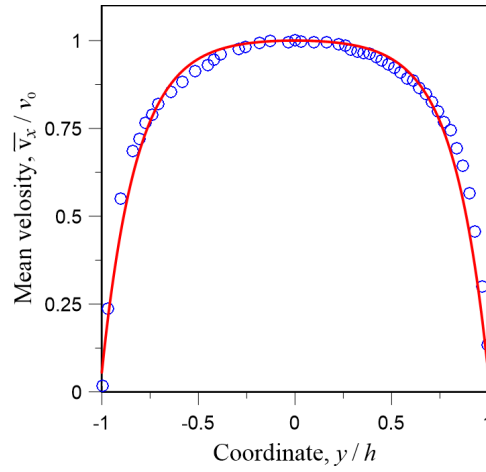


Figure 16: The distribution of mean velocity for plane Poiseuille flow. Experimental data are shown by circles (O) [17]. The solid red line corresponds to the profile (35) with $\lambda/h = 0.17$.

As an example, in Fig. 16 we demonstrate the fitting of the experimental velocity profile [17] by the normalized distribution (35). This figure shows the good agreement between the calculated profile and the experimental data.

7 Turbulent Poiseuille-Couette flow

Let us consider the combined Poiseuille-Couette flow in the channel, when one wall moves with speed v while the other one does not move (Fig. 17). We assume the fully developed turbulent flow, in which the vortex tubes on average rotate with a constant angular velocity $\bar{\omega}_z = \text{const}$, but with different phases $\bar{\varphi}_z(y)$.

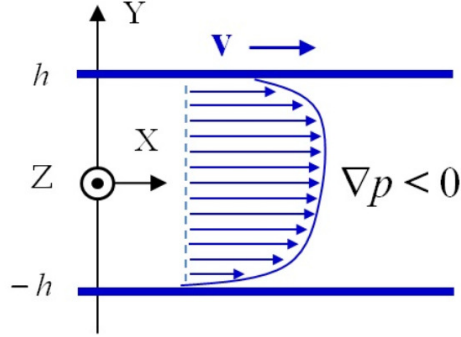


Figure 17: Sketch of a plane turbulent Poiseuille-Couette flow in a channel with one wall moving with speed v .

Let us look for a solution in the following form:

$$\begin{aligned}\bar{v}_x(y, t) &= \bar{v}_x(y), \\ \bar{\omega}_z(y, t) &= 2c\bar{\omega}_z t + \bar{\varphi}_z(y).\end{aligned}\tag{37}$$

In this case the equations (3) are rewritten as

$$\begin{aligned}-\lambda \frac{\partial^2 \bar{v}_x}{\partial y^2} + \frac{\partial \bar{\varphi}_z}{\partial y} - g &= 0, \\ -\lambda \frac{\partial^2 \bar{\varphi}_z}{\partial y^2} + \frac{\partial \bar{v}_x}{\partial y} + 2\bar{\omega}_z &= 0.\end{aligned}\tag{38}$$

We choose the following boundary conditions

$$\begin{aligned}\bar{v}_x(h) &= v, \\ \bar{v}_x(-h) &= 0, \\ \bar{\varphi}_z(h) &= \varphi_h, \\ \bar{\varphi}_z(-h) &= \varphi_{-h}.\end{aligned}\tag{39}$$

The solutions of these equations are

$$\begin{aligned}\bar{v}_x &= \frac{[2gh - (\varphi_h - \varphi_{-h})] [\cosh(h/\lambda) - \cosh(y/\lambda)]}{2 \sinh(h/\lambda)} \\ &+ v \left[\frac{\varepsilon y}{2h} + \frac{(1 - \varepsilon) \sinh(y/\lambda)}{2 \sinh(h/\lambda)} + \frac{1}{2} \right],\end{aligned}\tag{40}$$

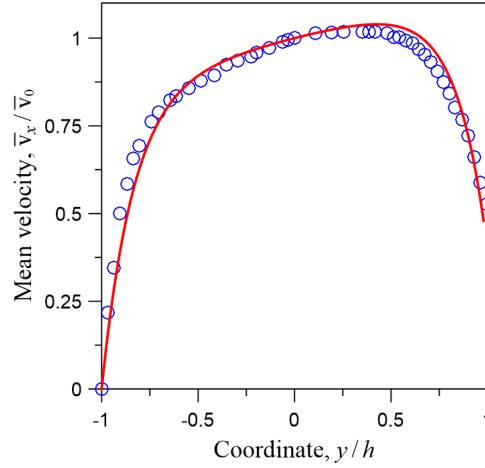


Figure 18: Distribution of mean velocity for Couette-Poiseuille flow in channel with moving wall. Circles (\circ) are experimental data [17], solid blue line corresponds to the profile (40) with $\xi = 0.006$, $\varepsilon = 0.65$, $\lambda/h = 0.155$.

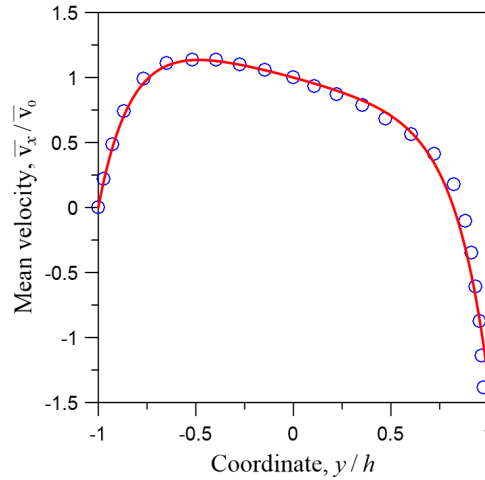


Figure 19: Distribution of mean velocity for Couette-Poiseuille flow in channel with wall moving in opposite to the flow. Circles (\circ) are the DNS data [19], solid blue line corresponds to the profile (40) with $\xi = 0.014$, $\varepsilon = 0.6$, $\lambda/h = 0.17$.

$$\begin{aligned} \bar{\varphi}_z = & -\frac{[2gh - (\varphi_h - \varphi_{-h})] \sinh(y/\lambda)}{2 \sinh(h/\lambda)} + gy \\ & + v \frac{(1 - \varepsilon) [\cosh(y/\lambda) - \cosh(h/\lambda)]}{\sinh(h/\lambda)} + \frac{\varphi_h + \varphi_{-h}}{2}, \end{aligned} \quad (41)$$

where we introduce the dimensionless parameter

$$\varepsilon = -\frac{4\bar{\omega}_z h}{v}. \quad (42)$$

To compare with experiment, we normalize the distribution (40) to the mean velocity at $y = 0$. As an example, Fig. 18 shows the correspondence between the velocity profile (40) and experimental data [17]. The dimensionless parameter $\xi = gh/v$ characterizes the relationship between the main flow velocity and the wall velocity. If the wall moves against the main flow, then in solution (40) the sign before the second term is changed. As an example, Fig. 19 shows the correspondence between the normalized velocity profile (40) and DNS data [19]. The figures 18 and 19 show that the calculated mean velocity profiles are in good agreement with the experimental data and the results of the DNS.

8 Concluding remarks

Thus, we have considered various types of plane steady-state turbulent flows within the simple model based on the equations describing the vortex motion of viscous fluid. In this model, the main parameter describing the characteristic spatial changes in the velocity profile is the turbulence scale λ , which is determined by the eddy viscosity of the flow [50].

In the case of near-wall turbulent flow over a flat plate, the parameter λ completely describes the velocity profile. The increase in velocity from 0 to v_∞ occurs asymptotically. However, to compare the model profiles with the experimental data published in the literature, we artificially introduced a boundary layer with the effective thickness δ . In this case, the parameter δ is the spatial scale on which the velocity increases, and the character of the mean velocity profile in the near-wall region is determined by the ratio λ/δ . This approach makes it possible to compare the results of model calculations with experimental data on velocity profiles in turbulent flows with low Reynolds numbers, as well as in a flow near the leading edge of a streamlined plate (see Fig. 6). However, to describe the flows with high Reynolds numbers, we had to complicate the model and take into account the averaged rotation of vortex tubes in the boundary layer. In this case, along with the parameter λ/δ , the velocity profile is described by an additional parameter β , which is determined by the ratio of the angular velocity of the tubes rotation to the main flow velocity. This allowed us to more accurately describe the velocity profiles for flows with high Re over a flat plate and over a plate with an obstacle (see Figs. 7 and 8).

The Couette and Poiseuille flows occur in a channel between two walls, and here an additional spatial scale, the channel width $2h$, appears naturally. Within our model the near-wall change in the Couette and Poiseuille velocity profiles is also determined by the turbulent length and depends on the parameter λ/h . This allowed us to qualitatively approximate the profile of the plane Poiseuille flow in the case of low Re (Fig.16). However, as the calculations showed, for a agreement between the model and experimental velocity profiles in the turbulent Couette flow, it is necessary to take into account the rotation of the vortex tubes. In this case, the additional parameter α (determined by the ratio of the angular velocity $\bar{\omega}_z$ and the wall velocity v) mainly controls the slope of the profile in the central region of the channel (Figs. 12 and 13). In addition, we have shown that the proposed simple model satisfactorily describes the velocity profiles of combined Poiseuille-Couette flows (Figs. 18 and 19). All calculated mean velocity profiles are in good agreement with the experimental data and the results of the DNS.

We believe that the proposed model of plane turbulent flows, based on the equations for vortex flows, can be used for a qualitative consideration of problems in hydrodynamics. Further extension of this model can be realized by considering composite flows and by varying the boundary conditions.

Acknowledgement

The authors are grateful to Galina Mironova for moral support.

References

- [1] M. Hansen, Die Geschwindigkeitsveileitung in der Grenzschicht an einer eingetauchten Platte, *Zeitschrift für Angewandte Mathematik und Mechanik*, 8(3) 185-199 (1928).
- [2] Z. Gete, R.L. Evans, An experimental investigation of unsteady turbulent-wake/ boundary-layer interaction, *Journal of Fluids and Structures* 17, 43–55(2003).
- [3] J.B.R. Loureiro, A.P. Silva Freire, Experimental investigation of turbulent boundary layers over steep two-dimensional elevations, *Journal of the Brazilian Society of Mechanical Sciences and Engineering*, 27(4), 329-344 (2005).
- [4] S. Sundeeep, H. Bu, P. Zhou, S. Zhong, X. Zhang, An experimental study of aerodynamic noise from large obstructions in turbulent boundary layer flows, *Physics of Fluids*, 34, 025121 (2022).
- [5] J. Jiménez, Near-wall turbulence, *Physics of Fluids*, 25, 101302 (2013).
- [6] H. Reichardt, Über die Geschwindigkeitsverteilung in einer geradigen turbulenten Couetteströmung, *Zeitschrift für Angewandte Mathematik und Mechanik*, 36, Sonderheft, 26-29 (1956).
- [7] E.M. Aydin, H.J. Leuthersser, Plane-Couette flow between smooth and rough walls, *Experiments in Fluids*, 11, 302312 (1991).
- [8] N. Tillmark, P.H. Alfredsson, Turbulence in plane Couette flow. In: *Advances in Turbulence IV* (ed. F.T.M. Nieuwstadt). *Fluid Mechanics and its Applications*, (Springer, Dordrecht), vol. 18, pp. 237-241 (1993).
- [9] N. Tillmark, P.H. Alfredsson, Experiments on transition in plane Couette flow, *Journal of Fluid Mechanics*, 235, 89-102 (1992).
- [10] K.H. Bech, N. Tillmark, P.H. Alfredsson, H.I. Andersson, An investigation of turbulent plane Couette flow at low Reynolds numbers, *Journal of Fluid Mechanics*, 286, 291325 (1995).
- [11] S. Bottin, H. Chate, Statistical analysis of the transition to turbulence in plane Couette flow, *The European Physical Journal B*, 6, 143-155 (1998).
- [12] O. Kitoh, K. Nakabyashi, F. Nishimura, Experimental study on mean velocity and turbulence characteristics of plane Couette flow: low-Reynolds-number effects and large longitudinal vortical structure, *Journal of Fluid Mechanics*, 539, 199–227 (2005).
- [13] M.M.M. El Telbany, A.J. Reynolds, Velocity distributions in plane turbulent channel flows, *Journal of Fluid Mechanics*, 100(1), 1-29 (1980).
- [14] S. Ansari, Md. A. I. Rashid, P.R. Waghmare, D.S. Nobes, Measurement of the flow behavior index of Newtonian and shear-thinning fluids via analysis of the flow velocity characteristics in a mini-channel, *SN Applied Sciences*, 2(11), 1787 (2020).

- [15] L. Wang, J. Mi, X. Meng, Z. Guo, A localized massconserving lattice Boltzmann approach for nonNewtonian fluid flows, *Communications in Computational Physics*, 17(4), 908 – 924 (2015).
- [16] L. Klotz, G. Lemoult, I. Frontczak, L. S. Tuckerman, J.E. Wesfreid, Couette-Poiseuille flow experiment with zero mean advection velocity: Subcritical transition to turbulence, *Physical Review Fluids*, 2, 043904 (2017).
- [17] E.M. Thurlow, J.C. Klewicki, Experimental study of turbulent Poiseuille–Couette flow, *Physics of Fluids*, 12, 865875 (2000).
- [18] K. Nakabayashi, O. Kitoh, Y. Katoh, Similarity laws of velocity profiles and turbulence characteristics of Couette–Poiseuille turbulent flows, *Journal of Fluid Mechanics*, 507, 43–69 (2004).
- [19] Q.T. Nguyen, D.V. Papavassiliou, Turbulent plane Poiseuille–Couette flow as a model for fluid slip over superhydrophobic surfaces, *Physical Review E*, 88, 063015 (2013).
- [20] O. Reynolds, On the dynamical theory of incompressible viscous fluids and the determination of the criterion, *Philosophical Transactions of the Royal Society of London*, A 186, 123–164 (1895).
- [21] W.D. McComb, Theory of turbulence, *Reports on Progress in Physics*, 58, 1117–1206 (1995).
- [22] F.S. Henry A.J. Reynolds, Analytical solution of two gradient-diffusion models applied to turbulent Couette flow , *ASME Journal of Fluids Engineering*, 106, 211–216 (1984).
- [23] K. Hanjalic, B.E. Launder, A Reynolds stress model of turbulence and its application to thin shear flows, *Journal of Fluid Mechanics*, 52 (4), 609–638 (1972).
- [24] P.S. Granville, Baldwin-Lomax factors for turbulent boundary layers in pressure gradients, *AIAA Journal*, 25(12), 1624–1627 (1987).
- [25] A. Mishra, S. Girimaji, Intercomponent energy transfer in incompressible homogeneous turbulence: multi-point physics and amenability to one-point closures, *Journal of Fluid Mechanics*, 731, 639–681 (2013).
- [26] S. Nisizima, A. Yoshizawa, Turbulent channel and Couette flows using an anisotropic k- model, *AIAA Journal*, 25(3) 414–420 (1987).
- [27] H.I. Andersson, B.A. Petterson, Modeling plane turbulent Couette flow, *International Journal of Heat and Fluid Flow*, 15(6), 447–455 (1994).
- [28] D.C. Wilcox, Formulation of the $k-\omega$ turbulence model revisited, *AIAA Journal*, 46 (11), 2823–2838, (2008),
- [29] H. Abe, H. Kawamura, Y. Matsuo, Direct numerical simulation of a fully developed turbulent channel flow with respect to the Reynolds number dependence, *ASME Journal of Fluids Engineering*, 123, 382–393 (2001).
- [30] T. Tsukahara, H. Kawamura, K. Shingai, DNS of turbulent Couette flow with emphasis on the large-scale structure in the core region, *Journal of Turbulence*, 7(19), 2006.
- [31] G.N. Coleman, S. Pirozzoli, M. Quadrio, P.R. Spalart, Direct numerical simulation and theory of a wall-bounded flow with zero skin friction, *Flow Turbulence Combust*, 99, 553–564 (2017).

- [32] J.H. Kim, J.H. Lee, Direct numerical simulation of a turbulent Couette–Poiseuille flow: Turbulent statistics, *International Journal of Heat and Fluid Flow*, 72, 288-303, (2018).
- [33] Y.K. Choi, J.H. Lee, J. Hwang, Direct numerical simulation of a turbulent plane Couette-Poiseuille flow with zero mean shear, *International Journal of Heat and Fluid Flow*, 90, 108836, (2021).
- [34] A. Sarkar, R.M.C. So, A critical evaluation of near-wall two-equation models against direct numerical simulation data, *International Journal of Heat and Fluid Flow*, 18, 197-208 (1997).
- [35] G. Gerodimos, R.M.C. So, Near-wall modeling of plane turbulent wall jets, *ASME Journal of Fluids Engineering*, 119, 304-313 (1997).
- [36] T. Kambe, A new formulation of equation of compressible fluids by analogy with Maxwell’s equations, *Fluid Dynamics Research*, 42, 055502 (2010).
- [37] R.J. Thompson, T.M. Moeller, Numerical and closed-form solutions for the Maxwell equations of incompressible flow, *Physics of Fluids*, 30, 083606 (2018).
- [38] C.R. Mendes, F.I. Takakura, E.M.C. Abreu, J. A. Neto, P.P. Silva, J.V. Frossad, Helicity and vortex generation, *Annals of Physics*, 398, 146-158 (2018).
- [39] H. Marmanis, Analogy between the Navier-Stokes equations and Maxwell’s equations: Application to turbulence, *Physics of Fluids*, 10, 1428-1437 (1998).
- [40] S. Demir, M. Tanişli, Spacetime algebra for the reformulation of fluid field equations, *International Journal of Geometric Methods in Modern Physics*, 14, 1750075 (2017).
- [41] M. Tanişli, S. Demir, N. Sahin, Octonic formulations of Maxwell type fluid equations, *Journal of Mathematical Physics*, 56, 091701 (2015).
- [42] S. Demir, A. Uymaz, M.Tanişli, A new model for the reformulation of compressible fluid equations, *Chinese Journal of Physics*, 55(1), 115-126 (2017).
- [43] R.J. Thompson, T.M. Moeller, A Maxwell formulation for the equations of a plasma, *Physics of Plasmas*, 19, 010702 (2012).
- [44] S. Demir, E. Zeren, Multifluid plasma equations in terms of hyperbolic octonions, *International Journal of Geometric Methods in Modern Physics*, 15(4), 1850053 (2018).
- [45] B.C. Chanyal, Quaternionic approach on the Dirac–Maxwell, Bernoulli and Navier– Stokes equations for dyonic fluid plasma, *International Journal of Modern Physics A*, 34(31) 1950202 (2019)
- [46] H. Helmholtz, Über Integrale der hydrodynamischen Gleichungen, welche den Wirbelbewegungen entsprechen, *Journal für die Reine und Angewandte Mathematik*, 55, 25—55 (1858).
- [47] V.L. Mironov, S.V. Mironov, Generalized sedeonic equations of hydrodynamics, *European Physical Journal Plus*, 135(9), 708 (2020).
- [48] V. L. Mironov, Self-consistent hydrodynamic two-fluid model of vortex plasma, *Physics of Fluids*, 33(3), 037116 (2021).

- [49] V.L. Mironov, Self-consistent hydrodynamic model of electron vortex fluid in solids, *Fluids*, 7, 330 (2022).
- [50] V.L. Mironov, S.V. Mironov, Vortex model of plane Couette flow, *Fluids*, 8(6), 165 (2023).
- [51] J. Boussinesq, Essai sur la th´eorie des eaux courantes, M´emoires pr´esent´es par divers savants a` l'Acad´emie des Sciences, 23(1), 1-680 (1877).
- [52] F.G. Schmitt, About Boussinesq's turbulent viscosity hypothesis: historical remarks and a direct evaluation of its validity, *Comptes Rendus M´ecanique*, 335(9-10), 617-627 (2007).
- [53] H. Schlichting, *Boundary Layer Theory*, 7th Edition. McGraw-Hill Inc., New York, 1979.
- [54] T. Tsukahara, H. Kawamura, K. Shingai, DNS Database of Wall Turbulence and Heat Transfer, Cou3000 A.dat, (<https://www.rs.tus.ac.jp/t2lab/db/>).
- [55] H. Kawamura, K. Shingai, Y. Matsuo, DNS Database of Wall Turbulence and Heat Transfer, Cou12800 A.dat, (<https://www.rs.tus.ac.jp/t2lab/db/>).